J. Fluid Mech. (1973), *vol.* 57, *part* 2, *pp.* 209–228
Printed in Great Britain

Pressure distributions on circular cylinders at critical Reynolds numbers

By J. P. BATHAM
Central Electricity Research Laboratories, Leatherhead, Surrey

(Received 11 September 1972)

Measurements have been made of the mean and fluctuating pressure distributions on long circular cylinders, having smooth and rough surfaces, at Reynolds numbers of $1{\cdot}11 \times 10^5$ and $2{\cdot}35 \times 10^5$ in both uniform and turbulent streams. The presence of free-stream turbulence at these Reynolds numbers was found to suppress coherent vortex shedding on the smooth cylinder and give rise to a complex pressure field in which the mean pressure distribution was almost independent of Reynolds number over the small range of Reynolds numbers tested. The pressure distributions on the rough cylinder were found to be completely different in uniform and turbulent streams; the presence of turbulence gave rise to an increase in the level of vortex shedding energy, and produced mean pressure distributions similar to those obtained on smooth cylinders at Reynolds numbers of the order of 10^7.

1. Introduction

This work is intended to provide further understanding of the parameters required for the wind-tunnel simulation of the mean and fluctuating pressures on tall chimneys. It is aimed at investigating the effects of Reynolds number, incident turbulence and surface roughness on the surface pressure distributions on circular cylinders. A long cylinder was chosen to enable the parameters under investigation to be isolated from the effect of finite cylinder length.

The work of Roshko (1961) demonstrated that the flow around a cylinder in the Reynolds number range 10^5–10^7 is a strong function of Reynolds number. As it is not possible to produce the Reynolds numbers corresponding to full-scale chimneys ($O(10^7$–$10^8)$) in existing wind tunnels at low Mach numbers, the possibility of simulating the correct pressure distribution by means of surface roughness at lower Reynolds numbers has been investigated.

2. Experimental equipment

2.1. *Details of the model*

The model consisted of a machined aluminium casting manufactured in three 0·23 m (9 in.) diameter sections with a total height of 1·53 m (5 ft). The two lower sections were assembled and mounted on the centre of the turntable of the C.E.R.L. $4{\cdot}59 \times 1{\cdot}53$ m Low-Speed Wind Tunnel. The upper section was bolted

to the wind-tunnel roof and housed a bearing on which the lower two sections could rotate. The maximum step at the joints between the three sections produced by ovalness and lack of concentricity was 0·3 mm. The maximum gap between the rotatable and fixed portions was 0·2 mm and all joints were sealed with silicone grease to ensure that no efflux could take place through the model and into the tunnel. The smooth-model tests were conducted with the cylinder in the as-machined condition, no attempt being made to improve the surface finish, which was typical of medium-quality turning. For the rough-model tests the surface was painted with a thin adhesive varnish and a uniform layer of 0·5 mm diameter sand particles was applied.

The moveable lower part of the model was provided with 1·6 mm bore pressure tappings in the following arrays.

(*a*) A circumferential ring of 24 tappings at 15° intervals in the centre-plane of the model.

(*b*) Four vertical generators at 90° intervals each having 23 tappings at 50·8 mm intervals.

2.2. *Details of the turbulence grid*

The turbulence was produced by a square-mesh grid which spanned the tunnel section. The grid consisted of rectangular bars 3·2 mm thick by 88·9 mm wide bolted to T-section bars of the same thickness and frontal width. It had a mesh size of 0·51 m and was mounted 39·8 bar widths (3·53 m) from the leading generator of the model.

2.3. *Details of instruments*

Measurements of fluctuating pressures were made using S.E. Laboratories differential pressure transducers. The pipe lengths between the transducers and the pressure tappings varied from 12·7 mm to 63·5 mm. Mean pressure measurements were made using Debro & Schiltknecht water-tube manometers.

The pressure transducer output were processed on line by a Pace TR 20 analog computer patched to process the outputs of three pressure transducers. An analog low-pass filter was placed between the pressure transducer output and the data processing or recording equipment to remove that part of the signal associated with Helmholtz resonance of the transducer/pipe cavity. This filter gave a -3 dB cut-off frequency of 99 Hz for the transducer and filter system as a whole when compared with a standard Brüel & Kjaer microphone. The integration period for the calculation of variances and covariances on the TR 20 was 200 seconds, which gave repeatability of the variances to within $\pm 2\,\%$ and an accuracy of the correlation coefficients of $\pm 0{\cdot}04$. All the variances quoted in this paper were measured using the analog computer. Only a few correlation coefficients were evaluated on line; these were intended to serve as a check.

Analog data recordings were made on a 14-channel Sangamo 3500 series tape recorder. The bulk of the correlation coefficients were evaluated from these tape recordings on a Myriad digital computer with an empirically determined sample length of 175 seconds, giving approximately 5×10^4 samples per channel. The results agreed with the values obtained on the analog computer to within $\pm 0{\cdot}06$. A longer sample length would have given greater accuracy but was unacceptable owing to the increased amount of wind-tunnel running time which would have

been required. It was not possible to obtain variances from the results as the gains of the signal conditioning amplifiers on the inputs to the tape recorder were not calibrated.

Analog data recordings were also made on the Sangamo 3500 series tape recorder and analysed on a Honeywell 9300 analyser to give power spectral densities of the pressure and free-stream velocity fluctuations. A sample length of data of 600 seconds was required to give sufficient resolution of low frequencies.

Hot-wire measurements of the grid-produced turbulence were made with a linearized Thermo-Systems type 1054A constant-temperature anemometer.

3. Experimental results

3.1. *The grid-produced turbulence*

Measurements of the properties of the grid-produced turbulence were made at a position 39·8 bar widths downstream of the grid, and the results are as follows: $q = 3$ mm of water; u component r.m.s. intensity $= 0{\cdot}129 \pm 0{\cdot}005$ (corresponding to $Re = 1{\cdot}11 \times 10^5$); $L(u, y) = 0{\cdot}20D$ at both tunnel speeds, where L refers to the turbulence integral length scale and D refers to the cylinder diameter. The values of $L(u, x)$ obtained from estimates of the power spectral densities near zero frequency are $L(u, x) = 0{\cdot}50D$ at both tunnel speeds.

The r.m.s. intensity of the u component in the absence of the grid was 0·5 %, and the tunnel-wall static pressure r.m.s. fluctuations in the presence of the grid were less than 1 % mean dynamic head at full tunnel speed.

3.2. *Cylinder pressure distributions*

Tests were conducted in uniform and turbulent flows for smooth and rough cylinders. All four combinations were tested at Reynolds numbers of $1{\cdot}11 \times 10^5$ and $2{\cdot}35 \times 10^5$. Mean and r.m.s. pressure distributions ($\bar{C}_p$ and C'_p) are presented in figures 1–4.

All the data presented have been corrected for tunnel blockage (5 %) by the method of Allen & Vincenti (1944). The maximum corrections to the mean free-stream velocity and the mean pressure coefficient were respectively 1·4 % and 3 % of their values. Such a blockage correction assumes that the pressure distribution is independent of Reynolds number, and does not therefore compensate completely for flows where the drag coefficient is changing rapidly with Reynolds number; however, it is assumed to be adequate for the small corrections required in the present work.

The mean drag coefficients C_D were determined by integration of the mean pressure distributions, and are shown tabulated with the base pressure coefficients $\bar{C}_{pb}$ in table 1.

For the smooth model in the uniform stream it was difficult to maintain a steady tunnel speed, and the pressure distribution was found to be a function of cylinder orientation. The grid-produced turbulence stabilized the flow and the tunnel speed remained steady. The unsteadiness observed in the uniform stream could be attributed to the negative slope of the drag/speed characteristic of the cylinder in this Reynolds-number range. The rough model was seen, by

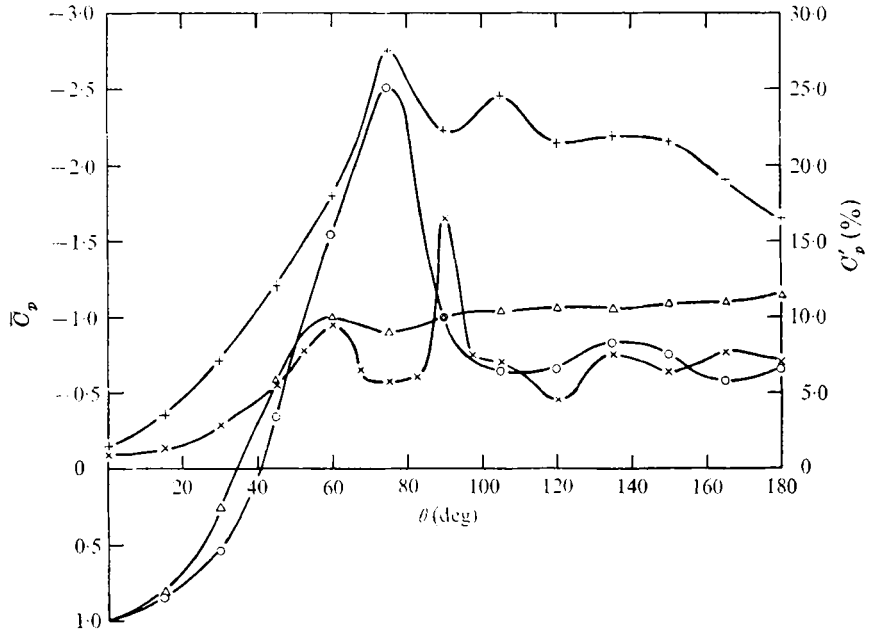

FIGURE 1. Distribution of $\overline{C}_p$ and C'_p on smooth cylinder in uniform stream. ×, C'_p, $Re = 2{\cdot}39 \times 10^5$; ○, $\overline{C}_p$, $Re = 2{\cdot}39 \times 10^5$; +, C'_p, $Re = 1{\cdot}11 \times 10^5$; △, $\overline{C}_p$, $Re = 1{\cdot}11 \times 10^5$.

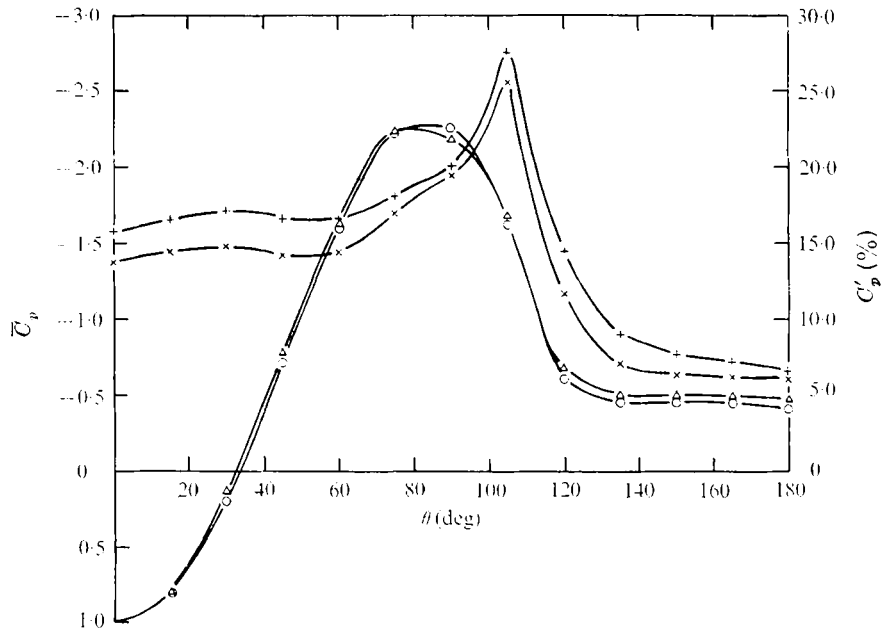

FIGURE 2. Distribution of $\overline{C}_p$ and C'_p on smooth cylinder in turbulent stream. ×, C'_p, $Re = 2{\cdot}35 \times 10^5$; ○, $\overline{C}_p$, $Re = 2{\cdot}35 \times 10^5$; +, C'_p, $Re = 1{\cdot}11 \times 10^5$; △, $\overline{C}_p$, $Re = 1{\cdot}11 \times 10^5$.

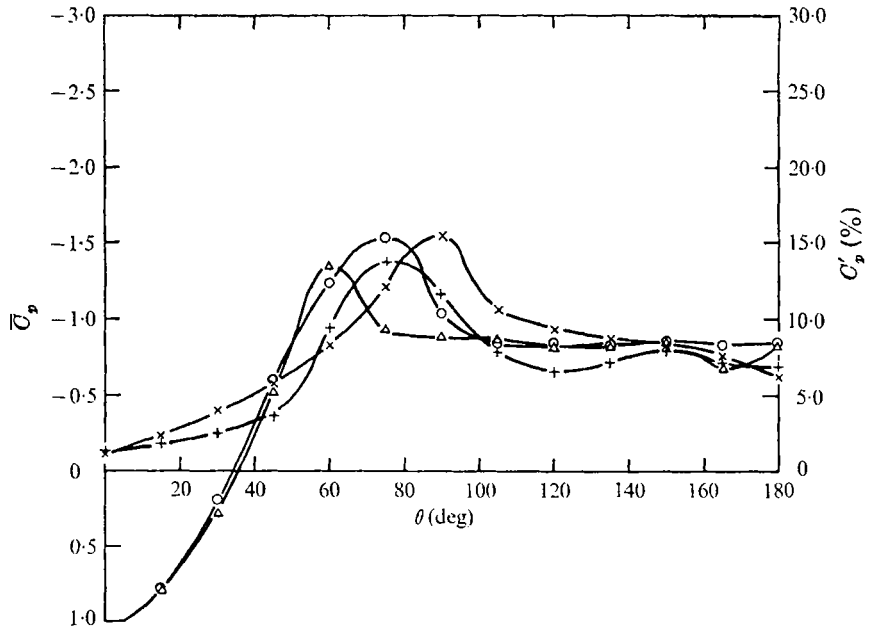

FIGURE 3. Distribution of $\overline{C}_p$ and C'_p on rough cylinder in uniform stream, ×, C'_p, $Re = 2{\cdot}35 \times 10^5$; ○, $\overline{C}_p$, $Re = 2{\cdot}35 \times 10^5$; +, C'_p, $Re = 1{\cdot}11 \times 10^5$; △, $\overline{C}_p$, $Re = 1{\cdot}11 \times 10^5$.

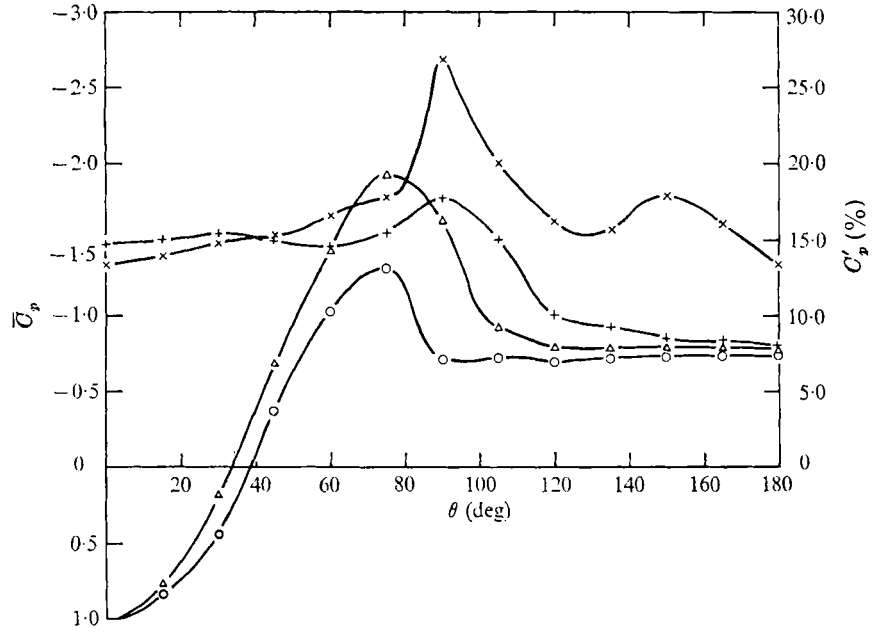

FIGURE 4. Distribution of $\overline{C}_p$ and C'_p on rough cylinder in turbulent stream, ×, C'_p, $Re = 2{\cdot}28 \times 10^5$; ○, $\overline{C}_p$, $Re = 2{\cdot}28 \times 10^5$; +, C'_p, $Re = 1{\cdot}11 \times 10^5$; △, $\overline{C}_p$, $Re = 1{\cdot}11 + 10^5$.

Stream	Model	Re	$\bar{C}_{pb}$	C_D
Uniform	Smooth	$1{\cdot}11 \times 10^5$	1·05	1·17
Uniform	Smooth	$2{\cdot}39 \times 10^5$	0·75	0·78
Turbulent	Smooth	$1{\cdot}11 \times 10^5$	0·50	0·41
Turbulent	Smooth	$2{\cdot}35 \times 10^5$	0·45	0·38
Uniform	Rough	$1{\cdot}11 \times 10^5$	0·83	0·72
Uniform	Rough	$2{\cdot}35 \times 10^5$	0·82	0·71
Turbulent	Rough	$1{\cdot}11 \times 10^5$	0·79	0·85
Turbulent	Rough	$2{\cdot}28 \times 10^5$	0·73	0·84

TABLE 1

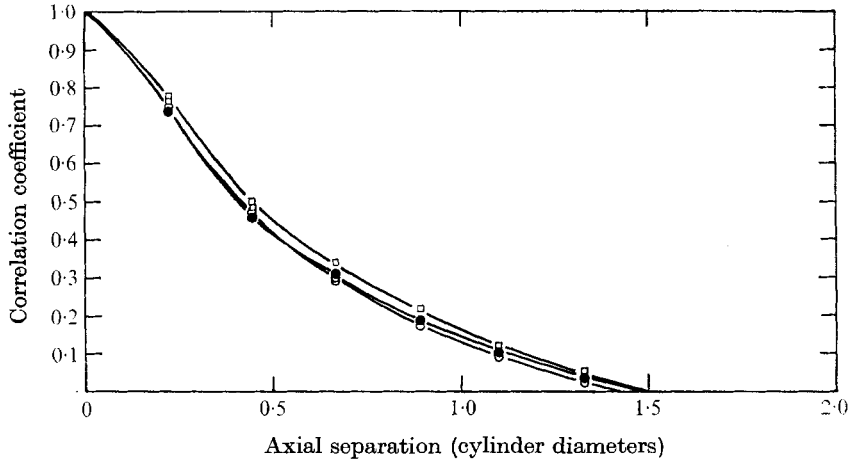

FIGURE 5. Axial correlation coefficients at leading generator for turbulent streams. ○, smooth cylinder, $Re = 2{\cdot}35 \times 10^5$, ●, smooth cylinder, $Re = 1{\cdot}11 \times 10^5$; □, rough cylinder, $Re = 2{\cdot}28 \times 10^5$.

observation of the pressure transducer output with an oscilloscope, to display coherent vortex shedding, and this was confirmed by spectral analysis. In this case the tunnel speed remained steady for both uniform and turbulent streams.

Axial and circumferential correlation coefficients of the surface pressure fluctuations were obtained at both Reynolds numbers for rough and smooth cylinders in uniform and turbulent streams. The axial correlations at the leading generator for turbulent streams are shown in figure 5 and the integral length scales of the correlations of the pressure fluctuations along a generator at various angles from the leading generator are shown in figures 6 and 7.

The fluctuating lift force and drag coefficients at one horizontal plane were evaluated from the expression

$$w' = \left[\iint a(\theta_1)a(\theta_2)\overline{p_1 p_2}\,d\theta_1 d\theta_2\right]^{\frac{1}{2}},$$

where $a(\theta)$ is $\sin\theta$ for lift-force evaluation and $\cos\theta$ for drag evaluation. The results are tabulated in table 2.

The distributions of $R(p;\theta,\alpha)$ as a function of α at various values of θ are shown in figures 8–12 for the most interesting cases. θ denotes the angle from the

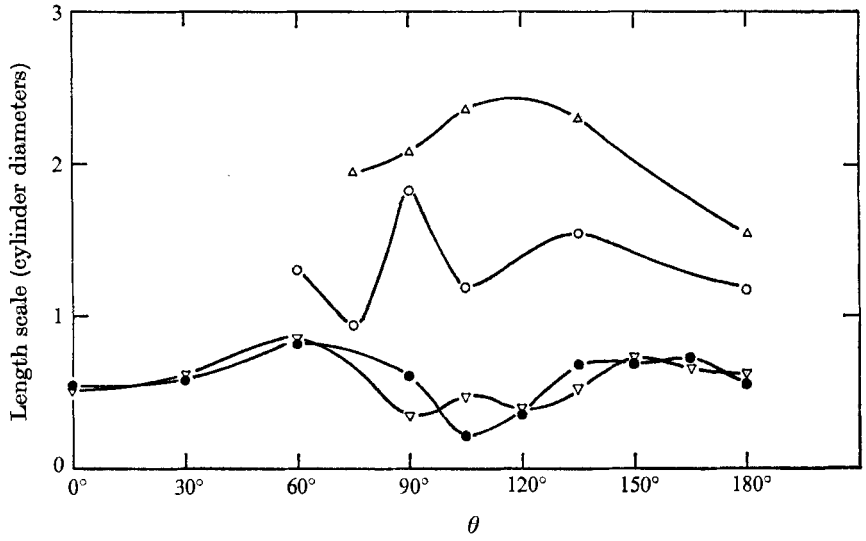

FIGURE 6. Axial length scales for smooth cylinder. ○, uniform stream, $Re = 2{\cdot}39 \times 10^5$; △, uniform stream $Re = 1{\cdot}11 \times 10^5$; ▽, turbulent stream, $Re = 2{\cdot}35 \times 10^5$; ●, turbulent stream $Re = 1{\cdot}11 \times 10^5$.

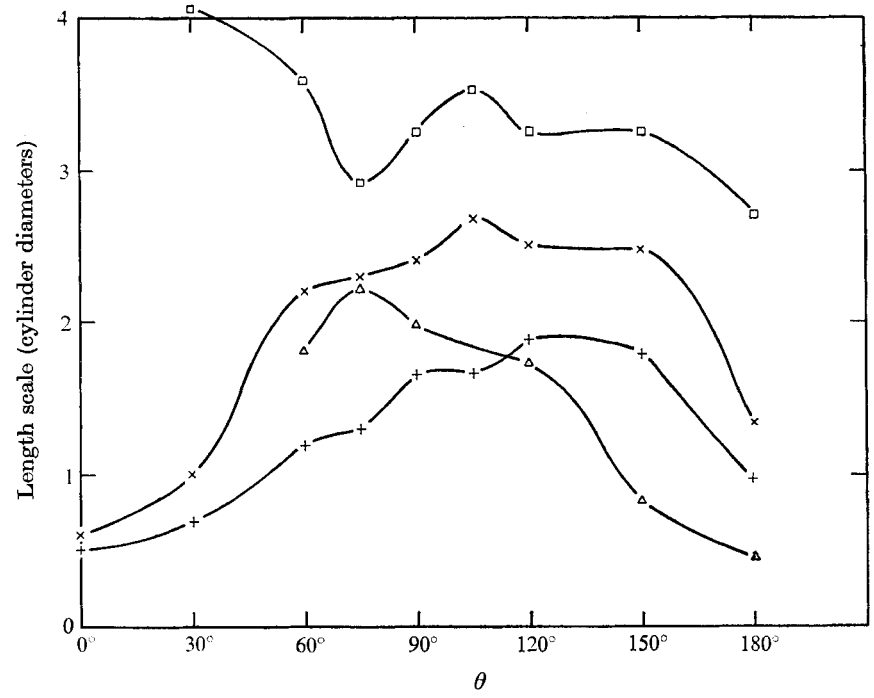

FIGURE 7. Axial length scales for rough cylinder. □, uniform stream, $Re = 2{\cdot}35 \times 10^5$; △, uniform stream, $Re = 1{\cdot}11 \times 10^5$; ×, turbulent stream, $Re = 2{\cdot}28 \times 10^5$; +, turbulent stream, $Re = 1{\cdot}11 \times 10^5$.

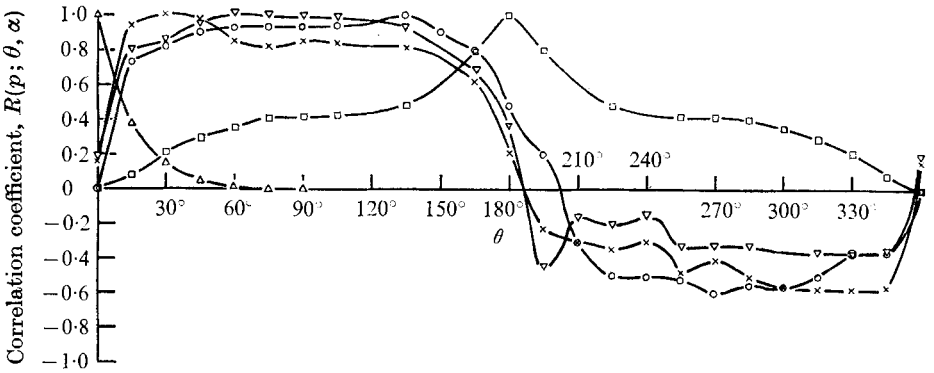

FIGURE 8. Distribution of $R(p;\theta,\alpha)$ for smooth cylinder in uniform stream at $Re = 1{\cdot}11\times10^5$. △, $\theta = 0°$; ×, $\theta = 30°$; ▽, $\theta = 60°$; ○, $\theta = 135°$; □, $\theta = 180°$.

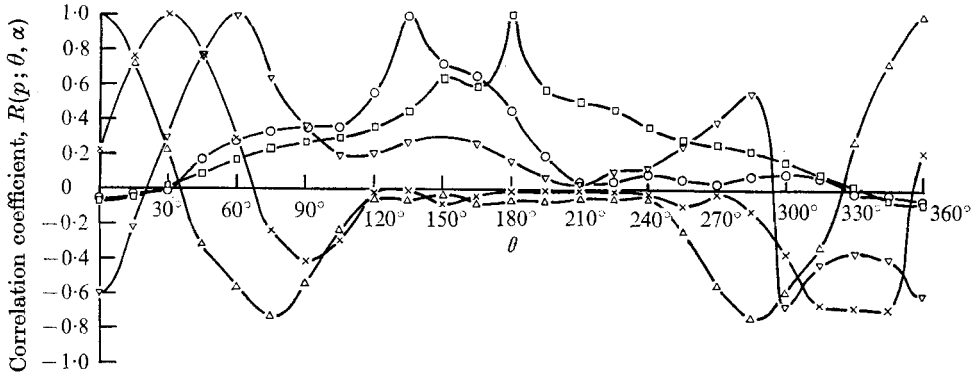

FIGURE 9. Distribution of $R(p;\theta,\alpha)$ for smooth cylinder in turbulent stream at $Re = 2{\cdot}35\times10^5$. △, $\theta = 0°$; ×, $\theta = 30°$; ▽, $\theta = 60°$; ○, $\theta = 135°$; □, $\theta = 180°$.

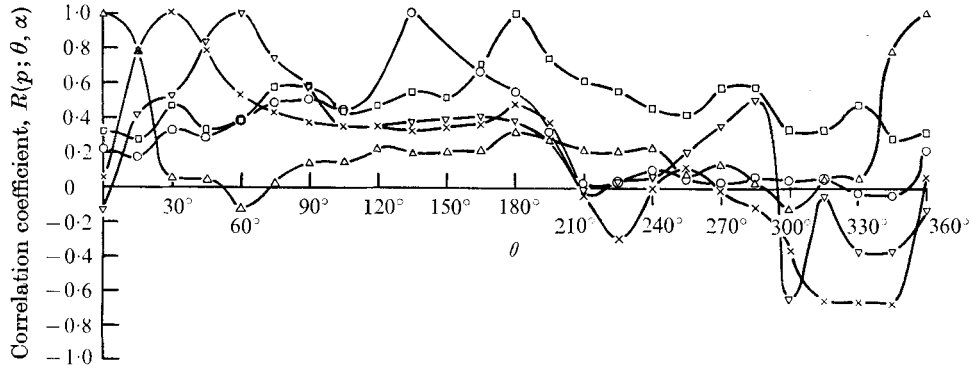

FIGURE 10. Distribution of $R(p;\theta,\alpha)$ for smooth cylinder in turbulent stream at $Re = 1{\cdot}11\times10^5$. △, $\theta = 0°$; ×, $\theta = 30°$; ▽, $\theta = 60°$; ○, $\theta = 135°$; □, $\theta = 180°$.

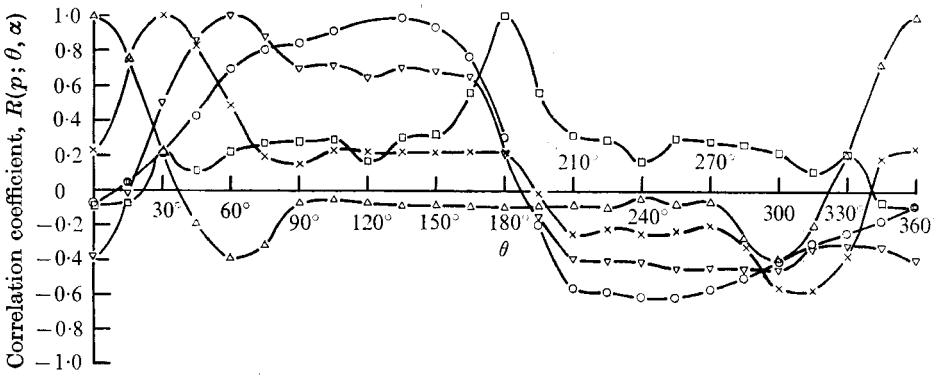

FIGURE 11. Distribution of $R(p;\theta,\alpha)$ for rough cylinder in turbulent stream at $Re = 2{\cdot}28\times10^5$. △, $\theta = 0°$; ×, $\theta = 30°$; ▽, $\theta = 60°$; ○, $\theta = 135°$; □, $\theta = 180°$.

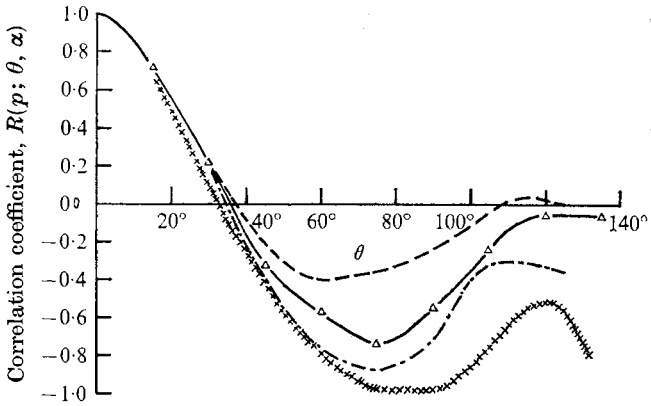

FIGURE 12. Distributions of $R(p;\theta,\alpha)$ with respect to the leading generator. – △ –, $L(u,x)/D = 0{\cdot}50$, turbulent–smooth, $Re = 2{\cdot}35\times10^5$; – – –, $L(u,x)/D = 0{\cdot}31$, turbulent–smooth (Tunstall); —·—, $L(u,x)/D \simeq 7$, Fawley full scale; × × × × $L(u,x)/D = \infty$, quasi-steady theory.

Stream	Model	Re	C'_L (%)	C'_D (%)
Uniform	Smooth	$1{\cdot}11\times10^5$	32·70	10·52
		$2{\cdot}39\times10^5$	8·79	4·06
Turbulent	Smooth	$1{\cdot}11\times10^5$	13·63	5·55
		$2{\cdot}35\times10^5$	9·05	6·90
Uniform	Rough	$1{\cdot}11\times10^5$	8·95	3·22
		$2{\cdot}35\times10^5$	15·01	3·72
Turbulent	Rough	$1{\cdot}11\times10^5$	15·30	7·18
		$2{\cdot}28\times10^5$	27·42	8·60

TABLE 2

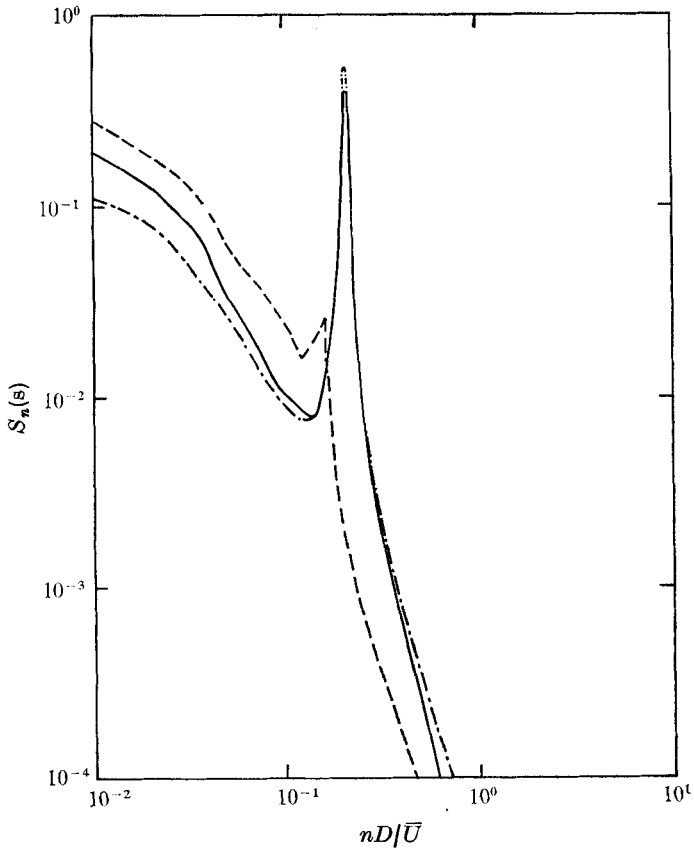

FIGURE 13. Power spectral density distributions of p for smooth cylinder in uniform stream at $Re = 2{\cdot}39 \times 10^5$. ——, $\theta = 60°$; – – –, $\theta = 75°$; —·—, $\theta = 90°$.

leading generator and α denotes the angular separation from the angle θ. $R(p; \theta, \alpha)$ denotes the correlation coefficient of fluctuating pressures between points at angles θ and α.

Power spectral densities of the pressure fluctuations at various values of θ are shown in figures 13–17. The power spectral densities S_n have been non-dimensionalized with respect to the total energy in each case, and are plotted with respect to the parameter $nD/\bar{U}$, where $\bar{U}$ is the mean velocity.

The spectra were obtained from the analog tape recordings of the pressure fluctuations using the Honeywell 9300 spectral analyser; as the frequency scale of the latter is accurate only to ± 5 %, the frequencies corresponding to the peaks in the spectra were determined more precisely by comparisons with spectra obtained using a calibrated frequency generator.

4. Discussion

4.1. *Smooth model in uniform stream*

At the lower Reynolds number the spectra show that a high level of vortex shedding was produced, giving rise to large values of C'_p downstream of the

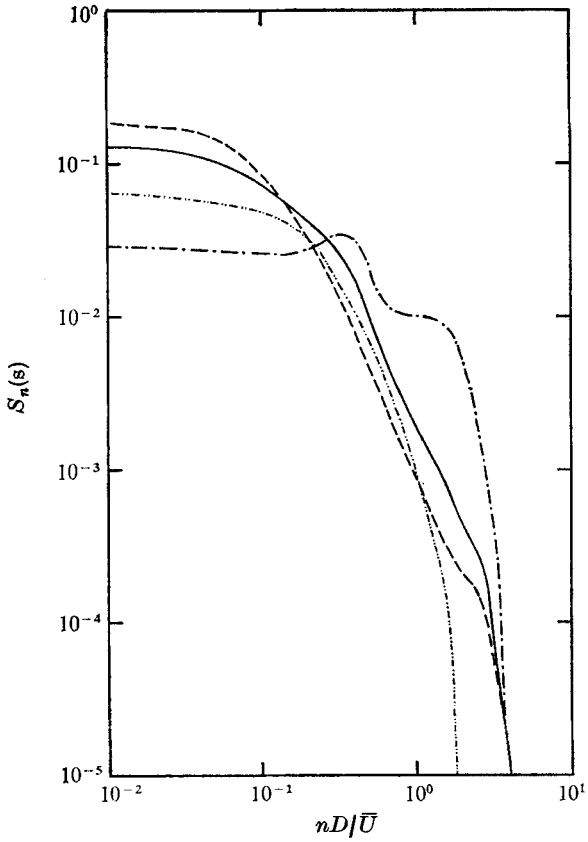

FIGURE 14. Power spectral density distributions of p for smooth cylinder in turbulent stream. ——, $\theta = 0°$, $Re = 1{\cdot}11 \times 10^5$; – – –, $\theta = 90°$, $Re = 1{\cdot}11 \times 10^5$; —·—, $\theta = 135°$, $Re = 1{\cdot}11 \times 10^5$; –· ·–, $\theta = 0°$, $Re = 2{\cdot}35 \times 10^5$.

separation point (see figure 8). The two peaks shown in the distribution of C'_p in figure 1 indicate the presence of a secondary separation bubble with a laminar separation and transitional reattachment. Son & Hanratty (1969) detected a secondary bubble on a nominally smooth cylinder in a uniform stream at a Reynolds number of 10^5 with the separation point at 77° from the leading generator. This separation location coincides within experimental accuracy with the first peak in the distribution of C'_p. The maximum pressure fluctuations at separation and reattachment may be caused by intermittent formation and collapse of the table. The secondary bubble was formed at a lower Reynolds number than that observed by Bearman (1969); the lower Reynolds number can be attributed to the greater surface roughness and free-stream turbulence used in the present work. No evidence was found of a Strouhal number of around 0·46 or a double shedding frequency as observed by Bearman, and it must be concluded that these results were peculiar to the combination of a highly polished cylinder and flow of low turbulence used by Bearman.

The peak at 60° in the distribution of C'_p at the higher Reynolds number, figure 1, does not appear to be due to an oscillating movement of the mean pressure

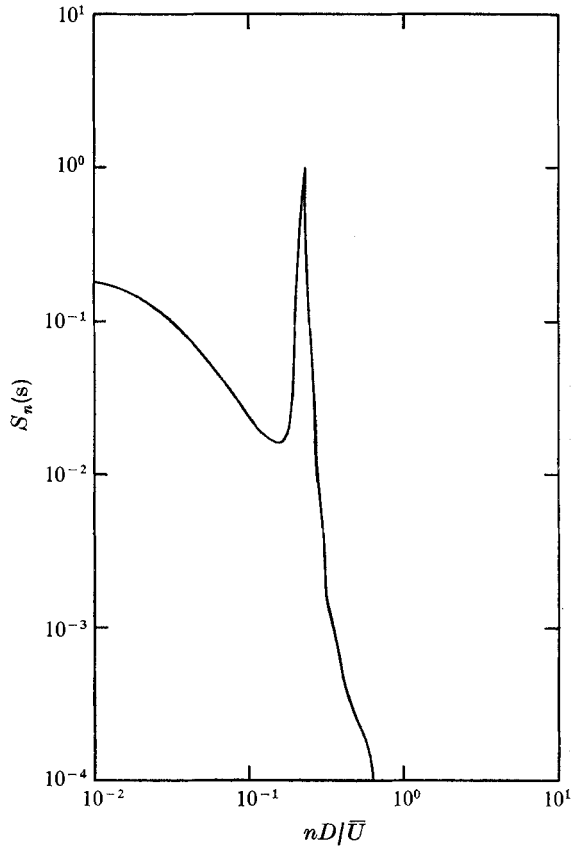

FIGURE 15. Power spectral density distribution of p for rough cylinder in uniform stream at $Re = 2{\cdot}35 \times 10^5$, $\theta = 120°$.

distribution, but to a change in the entire flow field as the cylinder was rotated. The spectra and distributions of C'_p were obtained from the output of a single transducer by rotating the cylinder, thus presenting a different distribution of local surface roughness to the flow. This variation in the roughness distribution could cause the entire flow pattern to be changed when the cylinder is rotated. It can be seen from the spectra (figure 13) that quite strong vortex shedding is observed at 60° and 90°, but very little at 75°, suggesting that the drop in the level of C'_p at 75° was due to a change in the type of flow around the cylinder. This view is supported by the highly scattered nature of the plot of axial correlation length scales for various values of θ as shown in figure 6. The flow at the lower Reynolds number exhibited a subcritical mean pressure distribution and would therefore not be expected to be highly sensitive to surface roughness. It is generally observed (E.S.D.U. 1970) that cylinders in uniform streams which exhibit critical mean pressure distributions are highly sensitive to surface roughness, which agrees with the above results.

The distribution of the mean pressure coefficient at the lower Reynolds number, figure 1, is in general agreement with that presented by Achenbach (1968) at the same Reynolds number on a polished cylinder in a stream of 0·7 % turbulence.

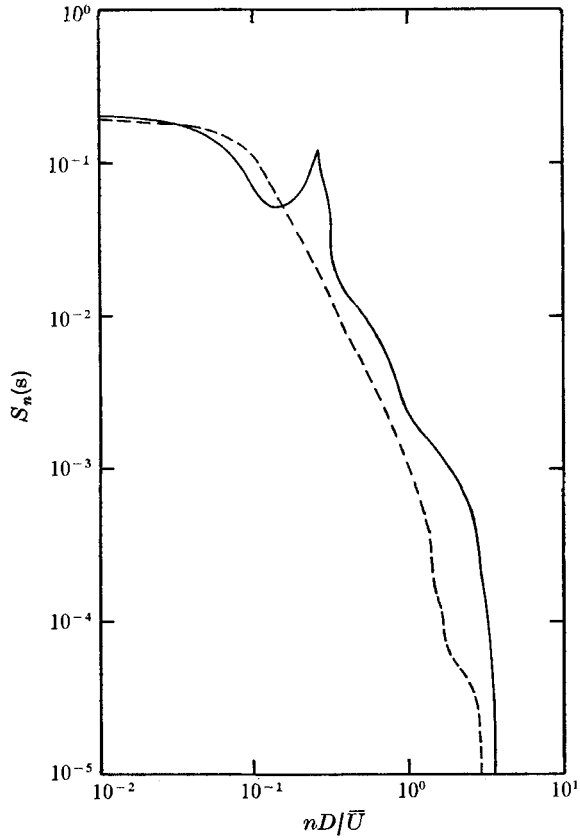

FIGURE 16. Power spectral density distributions of p for rough cylinder in turbulent stream at $Re = 1{\cdot}11 \times 10^5$. – – –, $\theta = 0°$; ——, $\theta = 120°$.

However, Achenbach's results show the magnitude of the peak suction to be greater, which would correspond to a higher Reynolds number in the C.E.R.L. tunnel. This would indicate that the high turbulence level employed by Achenbach promoted earlier transition in the shear layers and this effect was more pronounced than the effect of roughness on the attached boundary layer in determining the mean pressure distribution. However, the distribution of mean pressure coefficient at a Reynolds number of $2{\cdot}39 \times 10^5$ corresponds to Achenbach's results at a Reynolds number between $2{\cdot}6 \times 10^5$ and $8{\cdot}5 \times 10^5$, indicating that the effect of the greater surface roughness employed in the present work in promoting transition in the attached boundary layer was more important than the effect of free-stream turbulence at this Reynolds number. It is generally observed (E.S.D.U. 1970) that the critical range of Reynolds number is narrower for high roughness and wider for high turbulence; this agrees with the above observations.

The values of fluctuating lift and drag (table 2) at the lower Reynolds number fall within the data presented by Fung (1960). Fung's measurements are averages over a section with a length of about one axial length scale, whereas the measurements in the present work were taken at one horizontal plane. The correction for this effect is of the order of 20 %. The fluctuating lift at the higher Reynolds

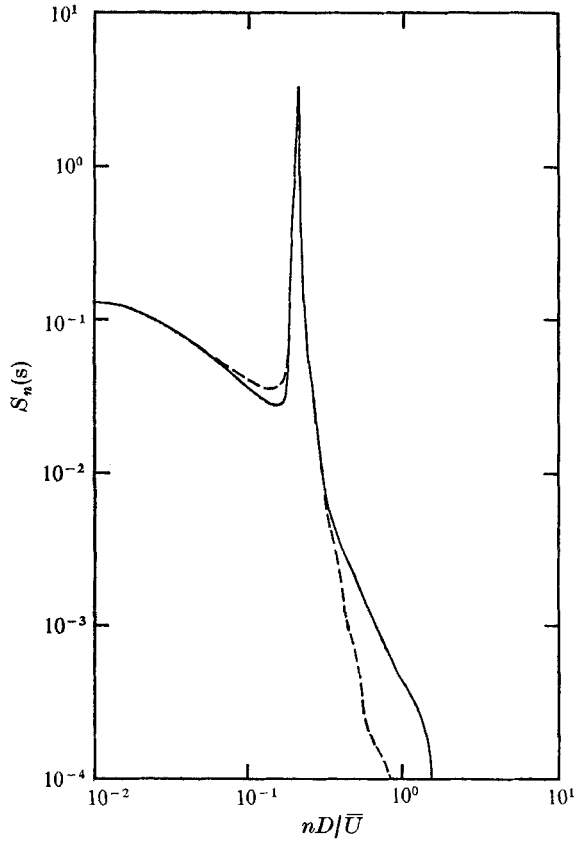

FIGURE 17. Power spectral density distributions of p for rough cylinder in turbulent stream at $Re = 2{\cdot}28 \times 10^5$. – – –, $\theta = 90°$; ——, $\theta = 150°$.

number is about 30 % lower than that reported by Fung, and could be due to the greater surface roughness employed in the present work promoting earlier transition and leading to a supression of vortex shedding. However, the fluctuating drag is in good agreement with Fung's data.

4.2. *Smooth model in turbulent stream*

The fluctuating pressure distribution around the front of the cylinder at the higher Reynolds number appears to be dominated by the incident turbulence. A negative lobe is shown in figure 9 in the distribution of $R(p; \theta, \alpha)$ with respect to the leading generator, as expected from the quasi-steady relation

$$C'_p = 2\frac{u'}{\bar{U}}\bar{C}_p + \frac{u'}{\bar{U}}\frac{\partial}{\partial\theta}\bar{C}_p,$$

where $u' = (\overline{u'^2})^{\frac{1}{2}}$. The negative lobe is also found in Tunstall's unpublished work on a long cylinder and by Tunstall's full-scale chimney measurements at Fawley Power Station (to be published). It can be seen in figure 12 that the moduli of the correlation coefficients are found to lie between those of Tunstall's cylinder and the Fawley results at angles of up to 105°, which would be expected as the

incident turbulence length scale to diameter ratio also lies between these two cases. The quasi-steady result, corresponding to an infinite length scale to diameter ratio, is seen to have an even greater modulus than the Fawley results, as expected. The peak in the negative lobe is located at 75°, compared with 60° on Tunstall's cylinder: the higher length scale to diameter and turbulence intensity employed in the present work would lead to a rearward movement of the peak, as wake fluctuations would not begin to give rise to a reduction in the magnitude of correlation until nearer the base region.

The negative lobe in the distribution of $R(p;\theta,\alpha)$ with respect to the leading generator is not found at the lower Reynolds number (figure 10), although it is observed at both Reynolds numbers on the rough cylinder in the turbulent stream, figure 11. There appears to be a higher level of correlation between points near the leading generator and points around the rear of the cylinder, see figures 9 and 10, implying that fluctuations in the wake region had a greater effect on the overall pressure distribution and produced the higher value of fluctuating lift coefficient calculated for this case (see table 2).

The gradual change in slope between low and high frequencies shown on the spectrum for $\theta = 0$ and $Re = 1{\cdot}11 \times 10^5$ (figure 14) appears to be caused by wake fluctuations influencing the flow around the front of the cylinder as indicated by the circumferential correlations (figure 10). At the higher Reynolds number a sharper cut-off is shown at $\theta = 0$, as was found also at the leading generator of the bluff aerofoil tested by Bearman (1972). At the higher Reynolds number the circumferential correlations (figure 9) show negligible correlation between the leading generator and the wake.

On a quasi-steady basis the value of C'_p at the leading generator should be equal to twice the incident free-stream turbulence intensity. However, the measured values of C'_p give values of 0·610 and 0·570 for $\bar{U}C'_p/2u'$, compared with the value obtained by Tunstall of 0·615, indicating that the turbulence length scale to diameter ratio has a negligible effect within the range considered. It can be seen from the slopes of the spectra of the pressure at the leading generator (figure 14) that the higher frequency fluctuations are more strongly attenuated than the well-established, $-\frac{5}{3}$ power law spectra of the incident turbulence. The values of the r.m.s. pressure fluctuations near zero frequency obtained from the spectra are 0·85 and 0·72 of the quasi-steady values at the lower and higher Reynolds numbers respectively, showing that quasi-steady theory gives incorrect results even at low frequencies.

An attempt to relate the skew correlations by separation of variables, i.e. $R(p;\alpha,\theta,z) = R(p;\theta,\alpha)R(p;\theta,z)$, gave errors of about 35 % at 30° from the leading generator and considerably larger errors at greater angles.

4.3. *Rough model in uniform stream*

The spectra show that a considerable proportion of energy due to coherent vortex shedding is produced at the higher Reynolds number. However, it can be seen from figures 3 and 4 that the distributions of $\bar{C}_p$ and C'_p are completely different for uniform and turbulent streams, indicating that the flow around the rough model in the uniform stream is not supercritical.

	Re	Roshko	Bearman
Universal number	—	0·163	0·181
Uniform–rough	$1{\cdot}11 \times 10^5$	0·145	0·164
Uniform–rough	$2{\cdot}35 \times 10^5$	0·182	0·172
Turbulent–rough	$1{\cdot}11 \times 10^5$	0·341	0·213
Turbulent–rough	$2{\cdot}28 \times 10^5$	0·214	0·184

TABLE 3

The separation point is located at about 75° at the lower Reynolds number for both the smooth–uniform and rough–uniform cases. However, the rough cylinder exhibits a considerably reduced level of vortex shedding, accompanied by a marked reduction in the levels of C'_p and fluctuating force coefficients (table 2). The long axial length scales shown in figure 7 suggest that the flow at separation was not highly three-dimensional, and it is suggested that processes of transition in the shear layers are responsible for the low level of coherent shedding and reduction of axial length scales at the rear of the cylinder.

The separation point is observed to have moved considerably further back at the higher Reynolds number, see figure 3; this case shows a considerably increased level of vortex shedding compared with that at the lower Reynolds number. The increased vortex shedding is accompanied by an increase in the ratio of fluctuating lift to fluctuating drag, with nearly antisymmetric distributions of $R(p;\theta,\alpha)$ as expected from the high level of vortex shedding. This would indicate that transition commenced further forward on the cylinder and enabled a higher adverse pressure gradient to be sustained before separation. The fact that transition was nearly complete at the separation point and the boundary layer more homogeneously turbulent would account for the higher level of vortex shedding observed.

The Strouhal numbers of vortex shedding were 0·18 and 0·23, which are within the range of those found for subcritical Reynolds numbers. Roshko (1961) observed a shedding Strouhal number of about 0·27 at Reynolds numbers between $3{\cdot}5 \times 10^6$ and $8{\cdot}5 \times 10^6$ on a smooth cylinder in uniform flow. 'Universal' Strouhal numbers have been proposed by Roshko (1954) and Bearman (1967), and it can be seen from table 3 that the frequencies produced in the present work show reasonable agreement. Generally Bearman's universal Strouhal number seems to agree with these measurements better than Roshko's.

4.4. *Rough model in turbulent stream*

The level of C'_p (figure 4) around the front of the cylinder is seen to be approximately constant up to the approach of separation at both Reynolds numbers. After separation the distribution at the lower Reynolds number is seen to fall to the level observed on the rough cylinder in the uniform flow but at the higher Reynolds number the distribution is similar to that shown on a rough cylinder in turbulent flow at a Reynolds number of $7{\cdot}1 \times 10^5$ tested by Tunstall (unpublished). A second peak in the region of 150° is observed, and is possibly associated with the increase in the higher frequency energy at this angle shown on the spectra in figure 17.

The distribution of $\bar{C}_p$ is also similar to that of Tunstall's results at the higher Reynolds number, but the high level of peak suction at the lower Reynolds number indicates a transitional separation flow. Tests on model cooling towers by Armitt (1968) have shown that, for roughness Reynolds numbers (Reynolds number based on surface roughness diameter) greater than about 600, the pressure distribution appears to be independent of free-stream turbulence. The cooling towers used by Armitt would have had a three-dimensional flow which would have tended to promote transition and also had some separation locations fixed by the lip at the top of the tower. Both these effects would have tended to give a reduction in the effect of incident turbulence. The roughness Reynolds number in the present case was 507, being the highest attainable at maximum wind-tunnel speed. The flows encountered in the present study fall into the region where Reynolds number, roughness Reynolds number and free-stream turbulence properties are all of significance in determining the flow and pressure fields. However, the similarity between the present high-Reynolds-number data and that of Tunstall indicates that the presence of free-stream turbulence was sufficient to promote transition to the extent that the boundary-layer flows were similar at separation.

The correlation lengths of the pressure fluctuations around the front of the cylinder at the lower Reynolds number are seen to be shorter than in the uniform-flow case (figure 7). This is due to the effect of the incident turbulence. Moreover, the higher level of coherent vortex shedding gave rise to longer length scales in the base region. In general the free-stream turbulence leads to a reduction in length scales compared with those of the uniform-flow case by adding a contribution to C'_p with small correlation lengths.

The distributions of $R(p;\theta,\alpha)$ shown, for example, in figure 11 are seen to display negative lobes in the correlations with respect to the leading generation at both Reynolds numbers. However, the amplitudes of the negative lobes are reduced compared with those for the smooth–turbulent case (see figure 12), indicating that wake fluctuations have some effect on the pressure distribution near the front of the cylinder. The axial correlations at the leading generator are shown in figure 5, and are observed to coincide with those obtained on the smooth cylinder in the turbulent stream.

5. General discussion of effects of turbulence and roughness

It has been shown by Naumann & Quadflieg (1968) that vortex shedding may be suppressed by the introduction of three-dimensionality into the boundary-layer flow upstream of separation for flow conditions which normally exhibit vortex shedding at Reynolds numbers close to the critical Reynolds number. Such three-dimensionality would be introduced into the flow near separation on a smooth cylinder by the action of incident turbulence leading to turbulent spot breakdown of the laminar boundary layer. The results of Schubauer & Klebanoff (1955) demonstrate that a transitional boundary layer on a smooth surface can be considered as a collection of turbulent spots which grow as they move downstream, finally merging to form a fully turbulent boundary layer.

Thus it would appear that, at Reynolds numbers close to the critical Reynolds number, the incident turbulence stabilizes the flow by promoting transition nearer to the leading generator, this effect dominating over the effect of local surface roughness. The boundary layer at separation will therefore consist of turbulent spots immersed in an unsteady laminar boundary layer, and will display a reduction in axial length scales as the number of turbulent bursts increases. It is generally found that turbulence has only a small effect on the second critical Reynolds number, at which the mean drag coefficient starts to increase, suggesting that free-stream turbulence lowers the Reynolds number for the start of transition but has little effect on the Reynolds number at the end of transition. The high skin-friction coefficient associated with a transitional boundary layer will enable a high mean adverse pressure gradient to be negotiated before separation as shown in figure 2.

It is suggested that the mechanism of transition may be slightly different on rough and smooth cylinders as the sand particles would tend to disperse turbulent bursts. This dispersal of the turbulent bursts would lead to transition taking place in a considerably shorter distance on a rough cylinder than on a smooth surface. It is generally observed that roughness has a considerably greater effect on the second critical Reynolds number than on the first critical Reynolds number, implying that the Reynolds number at which transition is complete is considerably reduced. This can be seen from the E.S.D.U. (1970) data sheet, which incorporates a correlation of all available data including the results given in this paper. Transition on a rough cylinder would be a more homogeneous process than is found on smooth cylinders and would not display the high skin-friction coefficient associated with turbulent bursts on a smooth surface. Thus the boundary layer on a rough surface would not be capable of withstanding such high mean adverse pressure gradients as on a smooth surface. Thus it is found that the minimum drag of rough cylinders is always higher than that of smooth cylinders, the value of minimum drag increasing with roughness until at very high roughness no minimum is observed at all. The more homogeneous nature of the boundary layer would enable a transitional boundary layer on a rough cylinder to exhibit vortex shedding which is not observed when transition is promoted by free-stream turbulence on a smooth cylinder.

A plot of peak mean suction against roughness Reynolds number was obtained by Armitt (1968) for model cooling towers, and is sketched in figure 18. It appears that the results obtained on the rough cylinder in the uniform stream were located before the peak shown on Armitt's curve as the peak suction is seen to increase with Reynolds number. The rough–turbulent results appear to be located on opposite sides of the peak as the distribution of C_p' at the lower Reynolds number is similar to the rough–uniform case downstream of separation, but the distribution at the higher Reynolds number is similar to Tunstall's results at a Reynolds number of $7{\cdot}1 \times 10^5$, at which free-stream turbulence has no effect on the mean pressure distribution. The general trend of the curves shown by Armitt can be explained with reference to the distribution of the skin-friction coefficient as a function of Reynolds number on a two-dimensional surface with zero or favourable pressure gradient. The ability of a boundary layer to pene-

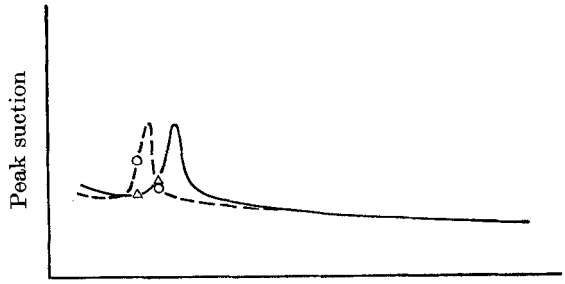

FIGURE 18. Peak mean suction/roughness Reynolds number of a cylindrical model. - - ○ - -, turbulent–rough; — △ —, uniform–rough.

trate an adverse pressure gradient without separation is a function of the velocity gradient at the wall, which also determines the skin-friction coefficient. It is well known that the skin-friction coefficient on a two-dimensional surface displays a peak near the end of transition, downstream of which the skin friction and boundary-layer velocity profile are weak functions of Reynolds number and are almost unaffected by free-stream turbulence. The peak of the mean suction on a cylinder is a function of the angular location of separation and the mean angle of the shear layers with respect to the free stream, both of which are determined by the state of the boundary layer at separation. Therefore the peak shown on Armitt's curve would correspond to the peak shown on the skin-friction distribution near the end of transition, after which Armitt's results show that peak suction is a weak function of Reynolds number and free-stream turbulence. The effect of free-stream turbulence is to promote transition nearer to the leading generator, thus giving rise to the peaks at lower Reynolds numbers.

6. Conclusions

The results obtained on the smooth cylinder in the uniform stream gave general agreement with previously published work. Local surface roughness was found to have a strong influence on the flow. The introduction of turbulence stabilized the flow and minimized the effect of local surface roughness, giving a mean pressure field which was a weak function of Reynolds number. It is suggested that the suppression of vortex shedding can be attributed to three-dimensionality and small axial correlations at separation caused by the presence of turbulent bursts. The flow in the region at the front of the cylinder in the turbulent streams was dominated by the incident turbulence for both smooth and rough cylinders.

The use of surface roughness was found to produce pressure distributions similar to those produced at Reynolds numbers of $O(10^7)$ on smooth cylinders when the incident stream was turbulent, but the pressure field was found to be completely different for uniform incident flows. These differences can be qualitatively explained with reference to the work of Armitt (1968) and suggest that processes of boundary-layer and shear-layer transition are dominant in determining the pressure field. Coherent vortex shedding of the correct frequency was observed

on the rough cylinders, but conclusions on the validity of the simulation of the amplitudes of the pressure fluctuations, associated with vortex shedding, by the use of roughness, cannot be drawn until high-Reynolds-number data are available.

This work was carried out at the Central Electricity Research Laboratories and is published by permission of the Central Electricity Generating Board.

REFERENCES

ACHENBACH, E. 1968 *J. Fluid Mech.* **34**, 625–639.

ALLEN, H. J. & VINCENTI, W. G. 1944 *N.A.C.A. Rep.* no. 782.

ARMITT, J. 1968 *Proc. Symp. on Wind Effects of Buildings and Structures*, paper 6. Loughborough University.

BEARMAN, P. W. 1967 *J. Fluid Mech.* **28**, 625–641.

BEARMAN, P. W. 1969 *J. Fluid Mech.* **37**, 577–585.

BEARMAN, P. W. 1972 *J. Fluid Mech.* **53**, 451–467.

E.S.D.U. 1970 *Engineering Sciences Data Item*, no. 70013. Engineering Sciences Data Unit.

FUNG, Y. C. 1960 *J. Aero. Sci.* **27**, 801–814.

NAUMANN, A. & QUADFLIEG, H. 1968 *Proc. Symp. of Wind Effects on Building and Structures*, paper 9. Loughborough University.

ROSHKO, A. 1954 *N.A.C.A. Tech. Note*, no. 3169.

ROSHKO, A. 1961 *J. Fluid Mech.* **10**, 345–356.

SCHUBAUER, G. B. & KLEBANOFF, P. S. 1955 *N.A.C.A. Rep.* no. 1289.

SON, J. B. & HANRATTY, T. J. 1969 *J. Fluid Mech.* **35**, 353–368.